ORIGINAL ARTICLE

Kinetic and mechanistic features on the reaction of stored TiO$_2$ electrons with Hg (II), Pb (II) and Ni (II) in aqueous suspension

Hanan H. Mohamed [a],*, Nuhad A. Alomair [b], Detlef W. Bahnemann [c,d]

[a] *Chemistry Department, Faculty of Science, Helwan University, Ain Helwan, 11719 Cairo, Egypt*
[b] *Department of Chemistry, College of Science, University of Dammam, P.O. Box 1982, Dammam 31441, Saudi Arabia*
[c] *Institut fuer Technische Chemie, Gottfried Wilhelm Leibniz Universitaet Hannover, Callinstrasse 3, D-30167 Hannover, Germany*
[d] *Saint-Petersburg State University, Laboratory "Photoactive Nanocomposite Materials", Saint-Petersburg 198504, Russia*

Abstract   The reaction of electrons stored on TiO$_2$ nanoparticles with heavy metal ions Hg (II), Ni (II) and Pb (II) has been studied employing steady state and stopped flow spectrophotometric techniques. Prior to kinetic investigation the formation of metal deposits is detected by their surface Plasmon absorbance observed after mixing of their corresponding metal ions with stored electron on TiO$_2$ nanoparticles (e$_{TiO_2}^-$). The dynamic of transfer of stored TiO$_2$ electrons to Hg (II), Pb (II) and Ni (II) in water has been investigated after mixing in the stopped flow chamber following the decrease of the absorbance of e$_{TiO_2}^-$ at 600 nm. The results indicate that Hg (II), Pb (II) and Ni (II) ions react readily with e$_{TiO_2}^-$. The kinetic parameters of the electron transfer reactions have been obtained by pseudo first order fitting. In the presence of Hg (II) ions, the transients decay followed by a buildup at 380–480 nm range. In the presence of Pb (II) and Ni (II), a concurrent decay of TiO$_2$ electron absorbance and buildup of the absorbance of metal deposits were observed. The rate constants of the electron transfer reactions induced by TiO$_2$ stored electrons to metal ions increase with the driving force of the reaction according to Tafel equation.

© 2016 Production and hosting by Elsevier B.V. on behalf of King Saud University. This is an open access article under the CC BY-NC-ND license (http://creativecommons.org/licenses/by-nc-nd/4.0/).

1. Introduction

Heavy metal ions in aquatic system such as Ni (II), Cu (II), Hg (II) and Pb (II) are common water pollutants that can damage our environment and cause many serious health problems. They inhibit many beneficial use of water since they interfere with functions of the vital cellular components of living organism's tissues (Jaerup, 2003; Salomons et al., 1995).

Various methods have been proposed for the treatment of wastewater containing metal ions such as chemical precipitation, ion exchange, electrolysis, adsorption and photocatalysis. Removal of

heavy metal ions from wastewater can effectively be carried out by photocatalysis (Chen and Ray, 2001; Litter, 2014). Photocatalytic removal of heavy metal ions from wastewater has been investigated using semiconductor nanoparticles such as TiO_2, ZnO and CdS (Litter, 2014, 1999; Nguyen and Beydoun, 2003; Legrini et al., 1993; Metcalf and Eddy Inc., 1991). Titanium dioxide has a good capacity to remove heavy metal ions by reducing them to their metallic forms which are relatively insoluble in water and nonpoisonous. The process of photocatalytic removal of heavy metal ions is rather simple. An ultraviolet radiation of wavelength less than 390 nm excites the conduction band electrons which subsequently trapped on the semiconductor surface (Kormann et al., 1988; Bahnemann et al., 1987). These trapped electrons can be used for metal ions reduction as the hole scavenged by organic molecules such as methanol.

Photocatalytic applications employing UV irradiated TiO_2 nanoparticles for removal of hazardous metal ions in aqueous solutions have been extensively studied during the past decades; however, less attention has been paid to the study of the kinetics and the mechanisms of these processes. This knowledge however is very important for the understanding and the industrialization of wastewater contaminants. The photocatalytic reduction of the metal ions by TiO_2 nanoparticles can be presented by the following equation:

$$M^{n+} + n e^-_{TiO_2} \rightarrow M^0 \tag{1}$$

One of the most important parameters that affect the efficiency of the photocatalytic removal of metal ions is their standard redox potential compared to the flat band potential of the TiO_2 nanoparticles since the metal ions of more positive reduction potentials than the TiO_2 band potential can only be photoreduced.

In our recent studies, the dynamics of $e^-_{TiO_2}$ transfer to various acceptors such as O_2, H_2O_2, NO^{3-}, Cu^{2+}, Zn^{2+}, Mn^{2+}, Ag^+ and Au^{3+} has been investigated in detail employing stopped flow technique (Mohamed et al., 2011a,b,c, 2012). It was found that while Zn^{2+} and Mn^{2+} ions cannot be reduced by TiO_2 electrons due to their thermodynamic infeasibility, the other acceptors reacted easily with stored TiO_2 electrons. The kinetics of the electron transfer from TiO_2 nanoparticles to Cr (VI) has been also investigated employing the same technique (Meichtry et al., 2015). The stopped flow spectrophotometric technique was found to be very powerful tool for such comprehensive and detailed study of the kinetics and mechanisms for electron transfer reactions with half lives as short as a few milliseconds.

In this paper the kinetics and the mechanisms of photocatalytic reduction of a variety of hazardous metal ions such as Hg (II), Ni (II), and Pb (II) using the stored electrons on the TiO_2 surfaces and employing the stopped flow technique have been studied. Furthermore, the growth of the corresponding metal nanoparticles was investigated by their typical UV–vis absorption spectra. The kinetic parameters have been obtained by fitting with first order kinetics. The effect of O_2 gas on the deposited metal particles and the effect of the initial metal ion concentration on the electron transfer kinetics were discussed. The relationship between the electron transfer rate constant (K_{et}) and the driving force of the electron transfer reaction ($E^0_{(M^{n+}/M^0)} - E^0_{CB}$) was also investigated.

2. Experimental

2.1. Materials

The chemicals were purchased from Sigma-Aldrich Company with the highest purity and were used without further purification. Titan(IV)-isopropoxide ($Ti(OCH(CH_3)_2)_4$) (99.999%), 2-propanol (99.999%), methanol (99.99%). All metal salts were chlorides: $HgCl_2$ (99.99%), $NiCl_2$ (99.99%) and $PbCl_2$

(99.99%). All solutions were prepared with distilled water (resistivity = 18.2 Ω cm).

2.2. Preparation of TiO_2 nanoparticles

Transparent colloidal suspension of TiO_2 nanoparticles was prepared from organic precursor Titan(IV)-isopropoxide according to a method reported by Bahnemann et al. (1984). Briefly, 5 ml of titanium tetraisopropoxide dissolved in 15 ml 2-propanol followed by dropwise in addition to perchloric acid solution of pH 1.5. This mixture was stirred over night until it was virtually clear. The pH was changed to 2.7 by dialyses against pure water using a double dialysis membrane. After rotary evaporation at 25 °C of the TiO_2 suspension, off white shiny crystals were obtained, which can be re-suspended in pure water to obtain perfectly transparent TiO_2 nanoparticles suspension.

2.3. Storage of electrons on TiO_2 nanoparticles

Storing of electrons on TiO_2 nanoparticles was performed by illuminating 3 g l^- (3.2×10^{-2} M) of Argon saturated TiO_2 aqueous suspension for 2 h in the presence of 0.02 M methanol as a hole scavenger. The photoreactor used for illumination was glass reactor (100 ml) with a sealed silicon cap irradiated from the top by 6 W UV light (365 nm).

2.4. Kinetic measurements

The kinetic experiments were performed using SF-3 rapid mixing stopped flow spectrophotometer (200–700 nm) with 2 mm optical path cell and 0.5 ms dead time mixing. In a typical stopped flow experiment, a pre-illuminated freshly prepared nanosized TiO_2 aqueous suspension at pH 2.7 was injected in one of the stopped flow syringes and an Argon saturated aqueous metal ion (Hg (II), Pb (II), Ni (II)) solution was injected in the other syringe. After mixing the change in the absorbance with time is measured in the optical cell. The electron transfer rate constants were determined by following the decrease of the absorbance of $e^-_{TiO_2}$ while the kinetics of the growth of metal deposits were studied by following the buildup of the absorbance of deposited metals, i.e., the plasmonic bands of the nanosized metal particles. Unless otherwise stated, the measurements were carried out under anaerobic condition at room temperature. All stopped flow measurements were performed three times and the results were averaged with experimental error not exceeding 5%. The rate constants which define the reaction kinetics were obtained by fitting the data using Origin 8 software.
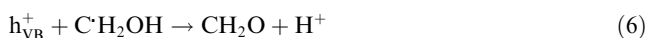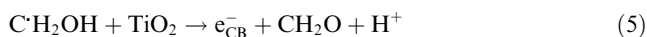
2.5. Analytical method

2.5.1. UV–vis absorption measurements
The absorbance spectra over a range of 200–800 nm were recorded employing a UV-1800 UV–vis spectrophotometer. The steady state UV–vis experiments have been performed by mixing an aqueous suspension of $e^-_{TiO_2}$ (4.62×10^{-4} M, 5 electrons/particle) with Ar-saturated aqueous metal ions solution (1×10^{-3} M) in a ratio of 1:1 in sealed cuvette.

3. Results and discussion

3.1. Storage of electrons on TiO$_2$ surfaces

The pre-illumination of degassed Argon purged aqueous system consisting of 3.2×10^{-2} M TiO$_2$ and 0.02 M methanol results in the formation of transparent blue suspension indicating the storing of electrons on TiO$_2$ nanoparticles (Mohamed et al., 2011a,b). This blue color was attributed to a broad absorption band in the region 400–800 nm according to the previous studies (Mohamed et al., 2011a). The blue color of illuminated TiO$_2$ suspension is due to Ti (III) species on the surface (Legrini et al., 1993; Metcalf and Eddy Inc., 1991). The initial concentration of stored electrons on TiO$_2$ was determined using the molar extinction coefficient $\varepsilon = 600$ M^{-1} cm^{-1} that has been reported in our previous work (Mohamed et al., 2011a,b). Assuming the determined ε value of TiO$_2$ electrons and that the particles of spherical shape of 4 nm size, the number of electrons per particle is found to range from 2 to 6 electrons per particle. The TiO$_2$ electron storing mechanism can be summarized as follows (Eqs. (2)–(6)):

$$TiO_2 \rightarrow TiO_2(e_{CB}^- + h_{VB}^+) \tag{2}$$

$$e_{CB}^- + Ti^{IV} \rightarrow Ti^{III} \tag{3}$$

$$h_{VB}^+ + CH_3OH_{ads} \rightarrow C\cdot H_2OH + H^+ \tag{4}$$

$$C\cdot H_2OH + TiO_2 \rightarrow e_{CB}^- + CH_2O + H^+ \tag{5}$$

$$h_{VB}^+ + C\cdot H_2OH \rightarrow CH_2O + H^+ \tag{6}$$

3.2. UV–vis measurements

The steady state UV–vis experiments have been performed by 1:1 mixing of the blue suspension of electrons loaded TiO$_2$ (4.62×10^{-4} M, 5 electrons/particle) at pH 2.7 with anoxic aqueous metal ions solutions ([M^{n+}] = 1×10^{-3} M, M^{n+} = Hg^{2+}, Pb^{2+}, Ni^{2+}) in a sealed cuvette. Since the reduction of the metal ions depends strongly on the presence of molecular oxygen, great care was taken to exclude molecular oxygen as far as possible during the manipulation of the solutions. Obviously, the broad absorption band (400–800 nm) of TiO$_2$ electrons decays immediately after mixing with metal ions solutions and new bands developed which are mostly assigned to the surface Plasmon absorbance of the corresponding metal nanoparticles.

3.2.1. Reaction of TiO$_2$ electrons with Hg (II)

The TiO$_2$ electrons spectrum was turned to yellow brown coloration after mixing with anoxic HgCl$_2$ aqueous solution. The spectra were recorded after mixing shows that the broad spectrum of TiO$_2$ electrons decayed and a featureless spectrum with a shoulder at 400–480 nm is observed (Fig. 1) confirming the two electrons reduction of Hg (II) into their corresponding Hg^0 particles followed by metal clusters growth (Eqs. (7) and (8)):
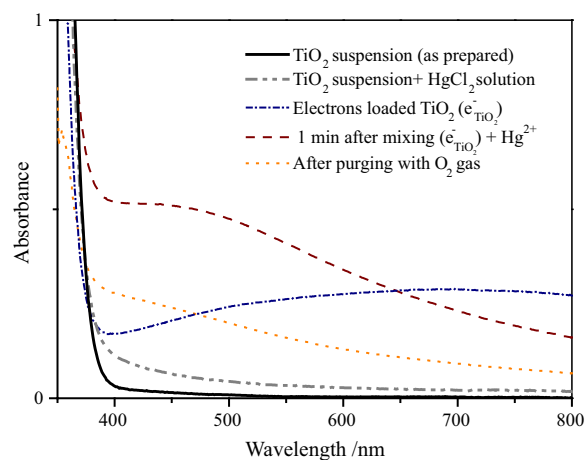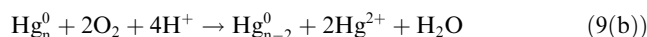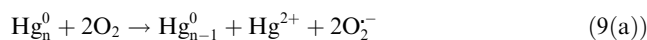
$$Hg^{2+} + 2e_{TiO_2}^- \rightarrow Hg^0 \tag{7}$$

Figure 1 UV–vis absorption measurements showing the absorbance spectrum of 3 g/l$^-$ as-prepared TiO$_2$ nanoparticles suspension (solid black line), as prepared TiO$_2$ suspension after mixing with Ar-saturated 1 mM HgCl$_2$ solution (dash dot gray line), stored TiO$_2$ electrons (e$_{TiO_2}^-$) (dot dash dot blue line), Hg^0 deposits absorption after mixing of e$_{TiO_2}^-$ (4.6×10^{-4} M, 5 e$_{TiO_2}^-$/TiO$_2$ particle) with an Ar-saturated aqueous solution of HgCl$_2$ ([Hg^{2+}] = 1 mM) (dashed wine line), and after purging final colloidal metal deposits with O$_2$ gas (dotted orange line). (For interpretation of the references to color in this figure legend, the reader is referred to the web version of this article.)

$$nHg^0 \rightarrow Hg_n^0 \tag{8}$$

It was reported previously that an aqueous suspension of Hg nanoparticles exhibits a broad maximum with an intense Plasmon absorbance band at 300 nm (Henglein and Giersig, 2000; Creighton and Eadon, 1991; Kapoor et al., 1999; Ketir et al., 2008). Under our experimental conditions it was not possible to detect the previously observed Plasmon band of Hg nanoparticles at 300 nm since under our experimental conditions TiO$_2$ particles absorbs strongly in this region though a broad absorption band at 400–480 nm was observed (Fig. 1) which can be attributed to the SP band of Hg nanoparticles. A blank experiment has been performed by 1:1 mixing of 3 g l^{-1} TiO$_2$ as prepared (before illumination) and 1×10^{-3} M HgCl$_2$ aqueous solution (Fig. 1). Obviously, no absorption bands have been observed in the wavelength range of interest evidences that the observed band at 400–480 nm after mixing e$_{TiO_2}^-$ and Hg^{2+} ions is attributed to SP band of Hg^0 nanoparticles. Interestingly, damping of Hg^0 spectra was observed immediately after purging with O$_2$ gas confirming their non stability toward molecular oxygen. This may be attributed to the oxidation of mercury particles giving back mercury ions and forming the corresponding reduced oxygen species (Eqs. 9(a) and 9(b)). Same phenomenon has been observed for Cu and Ag particles deposits on TiO$_2$ nanoparticles (Mohamed et al., 2011b,c):

$$Hg_n^0 + 2O_2 \rightarrow Hg_{n-1}^0 + Hg^{2+} + 2O_2^- \tag{9(a)}$$

$$Hg_n^0 + 2O_2 + 4H^+ \rightarrow Hg_{n-2}^0 + 2Hg^{2+} + H_2O \tag{9(b)}$$

3.2.2. Reaction of TiO₂ electrons with Pb (II)

A typical steady state UV–vis experiment was performed by mixing the aqueous electron suspension ($[e^-_{TiO_2}]$ = 5×10^{-4} M) with a deaerated aqueous PbCl$_2$ solution (1×10^{-3} M). The spectra are illustrated in Fig. 2. The transparent blue coloration of TiO$_2$ electron suspension turned to pale yellow coloration after mixing. A featureless spectrum is observed with increasing the absorbance in the shorter wavelength range which was growing with time. A blank experiment mixing the as prepared TiO$_2$ suspension before illumination with PbCl$_2$ solution shows no absorption band in the wavelength range 400–700 nm. Accordingly, the observed spectra after mixing $e^-_{TiO_2}$ and PbCl$_2$ solution are attributed to the Pb^0 particles and evidences the 2 electron reduction of Pb (II) into their corresponding metal particles (Eq. (10)). The surface Plasmon absorbance of lead nanoparticles has been investigated in previous studies as featureless spectrum with increasing the absorbance over 400 nm (Elango and Roopan, 2015). The absorption of Pb^0 particles cannot be observed above 400 nm under our experimental condition due to the strong absorbance of TiO$_2$ nanoparticles in this region.

$$Pb^{2+} + 2e^-_{TiO_2} \rightarrow Pb^0 \tag{10}$$

Similar to Hg^0 nanoparticles, damping of the spectra of the Pb^0 particles was observed after purging with O$_2$. This can be explained by oxidation of the metal deposits giving smaller particles in similar manner to Hg^0 deposits as described in Eqs. 9(a) and 9(b).
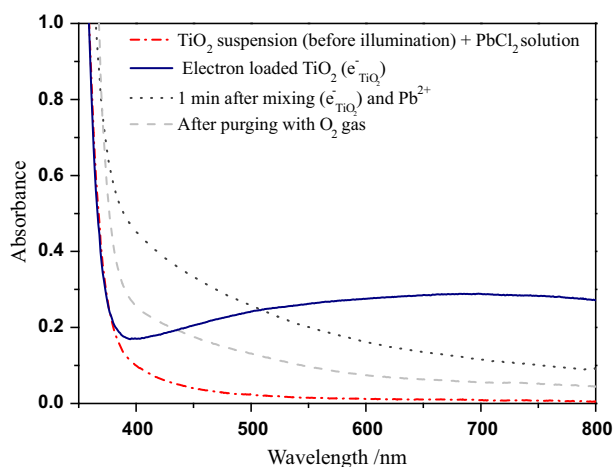
3.2.3. Reaction of TiO₂ electrons with Ni (II)

The TiO$_2$ electrons spectrum was turned to golden brown coloration after mixing with anoxic NiCl$_2$ aqueous solution (1×10^{-3} M). The spectra were recorded after mixing shows that the broad spectrum of TiO$_2$ electrons decayed and a broad spectrum with a shoulder at 500 nm is evolved (Fig. 3). The observed spectra can be attributed to the surface Plasmon band of Ni nanoparticles formed on the surface of TiO$_2$ nanoparticles which are close to the reported spectra (Meftah et al., 2009; Cardenas et al., 2001; Sadar et al., 2015). These observations confirm the two electrons reduction of Ni (II) into their corresponding Ni^0 particles (Eq. (11)):

$$Ni^{2+} + 2e^-_{TiO_2} \rightarrow Ni^0 \tag{11}$$

A strong damping of the absorption spectrum of Ni particles has been observed after purging with O$_2$ gas which can be readily explained by their oxidation.

3.3. Kinetic measurements

3.3.1. Stopped flow experiments with Hg (II)

The kinetics of the electron transfer reaction from TiO$_2$ electrons to Hg (II) was studied by following the decay of the TiO$_2$ electrons absorbance at 600 nm after mixing of electron loaded TiO$_2$ suspension ($[e^-_{TiO_2}]$ = 2.76×10^{-4} M, 2.8 $e^-_{TiO_2}$/particle) with various concentrations of Hg (II) solutions in absence of oxygen (Fig. 4(a)). Ar-saturated H$_2$O solution was used as blank. It was found that, while no absorbance decay at 600 nm was observed in absence of metal ions, a significant decay of TiO$_2$ electrons absorbance at 600 nm has been observed in the presence of Hg (II). A pseudo first order rate law was obeyed at all mercury ion concentrations. The
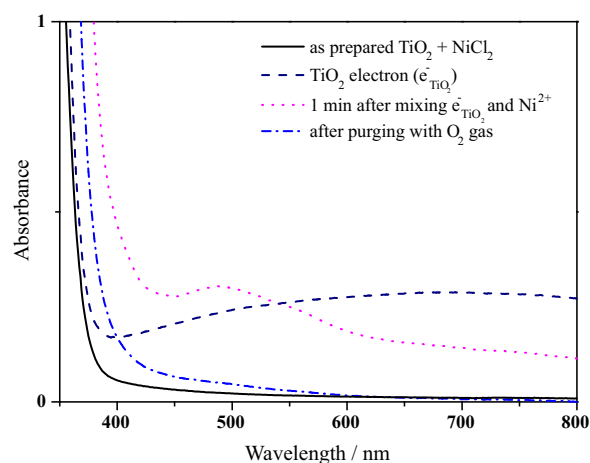

Figure 2 UV–vis measurements showing the absorption of 3 g l^{-1} as prepared TiO$_2$ (before illumination) with 1 mM PbCl$_2$ solution (1:1) (dashed dotted red line), the stored TiO$_2$ electrons absorbance (blue solid line), the Pb^0 deposits absorption after mixing of an aqueous suspension of TiO$_2$ electrons ($[e^-_{TiO_2}]$ = 4.6×10^{-4} M, 5 $e^-_{TiO_2}$/particle) with an Ar-saturated aqueous solution of Pb^{2+} (PbCl$_2$), [Pb^{2+}] = 1 mM (black dotted line) and after purging final colloidal metal deposits with O$_2$ gas (dashed gray line). (For interpretation of the references to colour in this figure legend, the reader is referred to the web version of this article.)

Figure 3 UV–vis measurements of the absorption of the as prepared TiO$_2$ suspension (3 g l^{-1}) after mixing with 2 mM NiCl$_2$ solution (1:1) (solid black line), stored TiO$_2$ electrons (Navy dashed line), Ni^0 deposits absorption after mixing of an aqueous suspension of TiO$_2$ electrons ($[e^-_{TiO_2}]$ = 4.6×10^{-4} M, 5 $e^-_{TiO_2}$/particle) with an Ar-saturated aqueous solution of Ni^{2+} (NiCl$_2$), [Ni^{2+}] = 2×10^{-3} M (dashed pink line) and after purging final colloidal metal deposits with O$_2$ gas (dashed dotted blue line). (For interpretation of the references to colour in this figure legend, the reader is referred to the web version of this article.)
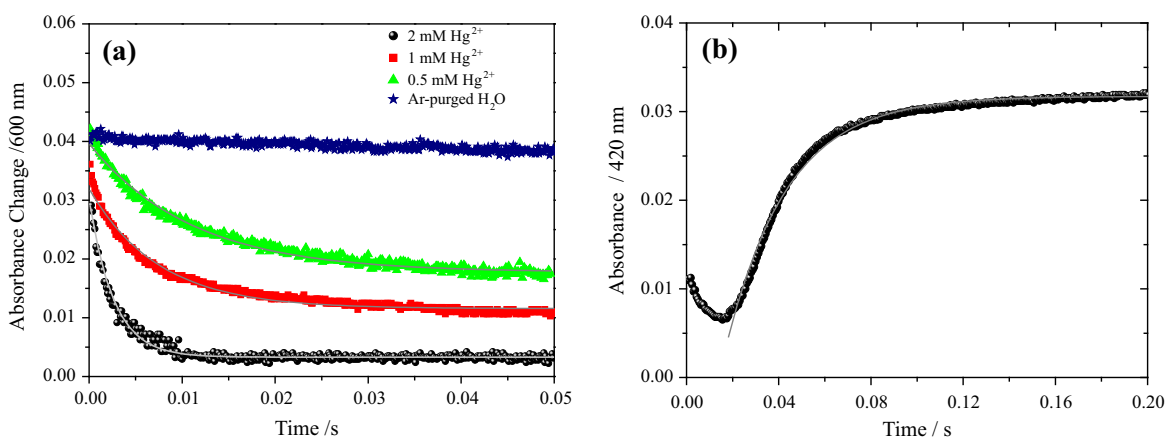
Figure 4 (a) Time profiles of the decay of the $e^-_{TiO_2}$ absorbance at 600 nm ([$e^-_{TiO_2}$] = 2.76 × 10^{-4} M, 2.8 $e^-_{TiO_2}$/particle) observed after mixing of their aqueous suspension with Ar-saturated aqueous HgCl$_2$ solutions with different concentrations and with Ar-saturated H$_2$O in absence of Hg ions at pH 2.7, solid lines show the first order fits. (b) Long timescale profile at 420 nm observed after mixing of stored TiO$_2$ electrons suspension ([$e^-_{TiO_2}$] = 2.76 × 10^{-4} M, 2.8 $e^-_{TiO_2}$/particle) with deaerated aqueous HgCl$_2$ solution ([Hg^{2+}] = 1 × 10^{-3} M) at pH 2.7, solid line shows data fitting (k^{obs} = 18.18).

first order rates were found to increase with Hg (II) concentrations. The first order rate constants are shown in Table 1. The observed second order rate constant of the two electron reduction of Hg (II) by TiO$_2$ stored electrons was obtained from the measurements at different concentrations to be k^{obs}_2 = 1.89 × 10^5 M^{-1} s^{-1}. Following the decay a buildup was observed at the wavelength range of 380–480 nm. Fig. 4 (b) shows a long scale time profile at 420 nm, and initially first order decay is observed followed by a transient absorbance buildup. The buildup rate depends on the concentration of Hg^0. Hence, the growth of Hg^0 deposits can be described by an autocatalytic process. The rate constant of Hg^0 growth was obtained by single exponential fitting to be k^{obs} = 18.18 s^{-1} at 1 mM of Hg (II).

3.3.2. Stopped flow experiments with Pb (II)

Fig. 5(a) shows the transients obtained at 600 nm and 420 nm after mixing Ar-purged 0.5 mM Pb^{2+} aqueous solution with 3 g l^{-1} TiO$_2$ suspension with 0.42 mM $e^-_{TiO_2}$. A significant decay of the signals at 600 nm has been observed. Simultaneously, a significant buildup of the signals at the wavelength range of 400–460 nm has been observed. From calculating the number of electrons consumed due to the absorbance decay, it was obvious that a 2 electron transfer process was found to take place which is proved by the steady state exper-

iment evidences the 2 electron reduction of Pb^{2+} ions to their metallic nanoparticles. The absorbance decay rate constants due to the reduction of Pb^{2+} were obtained by performing the kinetic experiments at different concentrations of Pb^{2+} ions. Fig. 5(b) shows the absorbance decays at 600 nm observed after mixing the electron loaded TiO$_2$ suspension with lead ions aqueous solutions at different concentrations. The transients decay as well as buildup could be adjusted to pseudo first order kinetics with good correlation coefficients ($R^2 \geqslant 0.96$). All the kinetic parameters are shown in Table 1.

3.3.3. Stopped flow experiments with Ni (II)

The transient absorbance at 600 nm and 420 nm obtained after mixing of electron loaded TiO$_2$ suspension ([$e^-_{TiO_2}$] = 5.89 × 10^{-4} M, 6.2 $e^-_{TiO_2}$/particle) with 2 mM aqueous solution of Nickel ions is shown in Fig. 6(a). A significant decay at 500–650 nm while a concurrent buildup at 400–480 nm has been observed. The kinetics of the electrons absorbance decay at 600 nm has been obtained at different concentrations of nickel ions (Fig. 6(b)). The kinetic curves were analyzed according to a single exponential fitting. The observed first order rate constants were found to increase with the concentrations of the Nickel ions. The kinetic parameters are shown in Table 1.

Table 1 Kinetic parameters obtained from first order fitting of the experimental points of Figs. 4–6.

Acceptor	Acceptor concentration/mM	Electron concentration/mM	k_1, s^{-1}	R^2
Hg^{2+}	2	0.277	384.62	0.98
Hg^{2+}	1	0.293	135.13	0.98
Hg^{2+}	0.5	0.342	91.07	0.97
Pb^{2+}	1	0.430	3.12	0.95
Pb^{2+}	0.5	0.420	1.75	0.92
Pb^{2+}	0.25	0.427	0.96	0.94
Ni^{2+}	2	0.59	3.54	0.95
Ni^{2+}	1	0.58	1.67	0.96
Ni^{2+}	0.5	0.59	0.88	0.94

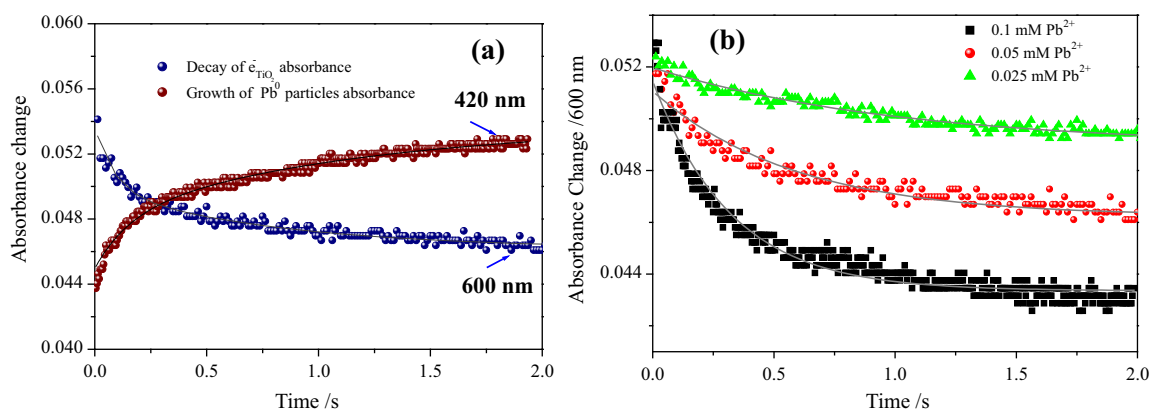**Figure 5** (a) Time profiles of the decay of the $e_{TiO_2}^-$ absorbance at 600 nm and the buildup at 420 nm observed after mixing of an aqueous TiO$_2$ electrons suspension ($[e_{TiO_2}^-]$ = 4.27 × 10^{-4} M, 4.5 $e_{TiO_2}^-$/particle) with Ar-saturated aqueous PbCl$_2$ solution (0.5 mM) at pH 2.7, (b) time profiles of the decay of the $e_{TiO_2}^-$ absorbance at 600 nm ($[e_{TiO_2}^-]$ = 4.27 × 10^{-4} M, 4.5 $e_{TiO_2}^-$/particle) observed after mixing of their aqueous suspension with Ar-saturated aqueous PbCl$_2$ solutions with different concentrations at pH 2.7, solid lines show the first order fits.
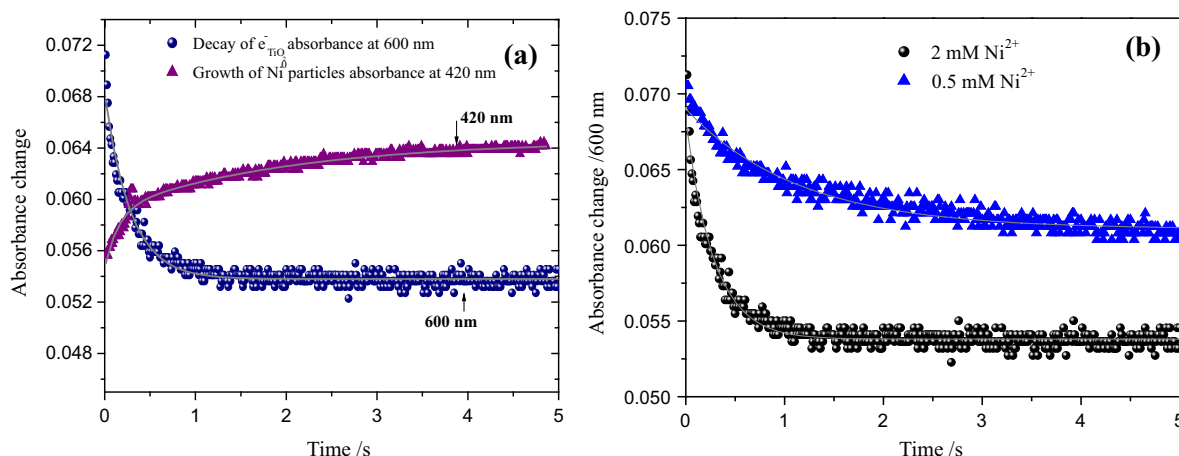

Figure 6 (a) Time profiles of the decay of the $e_{TiO_2}^-$ absorbance at 600 nm and the buildup at 420 nm observed after mixing of an aqueous TiO$_2$ electrons suspension ($[e_{TiO_2}^-]$ = 5.89 × 10^{-4} M, 6.2 $e_{TiO_2}^-$/particle) with Ar-saturated aqueous NiCl$_2$ solution (2 mM) at pH 2.7. (b) Transients decay at 600 nm at different Ni^{2+} concentrations.

Table 2 Summary of the electron transfer rate constants of the reaction of $e_{TiO_2}^-$ with heavy metal ions (Hg (II), Pb (II), Ni (II)), their corresponding reactions and the corresponding redox potentials.

Reaction	E^0 (V_{NHE})[25]	k_{obs}/M^{-1} s^{-1}	K_{et}/cm s^{-1}
Ni^{2+} + 2e$_{TiO_2}^-$ → Ni^0	−0.25	1.77 × 10^3	5.45 × 10^{-6}
Pb^{2+} + 2e$_{TiO_2}^-$ → Pb^0	−0.126	3.08 × 10^3	9.07 × 10^{-6}
Cu^{2+} + 2e$_{TiO_2}^-$ → Cu^0	+0.34	3.5 × 10^4	1.87 × 10^{-4} [12]
Hg^{2+} + 2e$_{TiO_2}^-$ → Hg^0	+0.85	1.89 × 10^5	5.68 × 10^{-4}

3.4. Relation between interfacial electron transfer rate constants and driving force

The efficiency of the photocatalytic reduction of transition metal ions is significantly affected by the value of standard redox potential of metallic couple compared to the redox potential of conduction band electron. The driving force of the reaction of electron transfer to metal ions can be defined as the difference between the standard redox potential of the metallic couple ($E^0_{(M^{n+}/M^0)}$) and that of the conduction band electrons corresponding to the Fermi energy (E^0_{CB}).

The changing of interfacial electron transfer rate constant K_{et} (cm s^{-1}) with the driving force $E^0_{(M^{n+}/M^0)} - E_{CB}$ can be described according to Tafel Equation (Eq. (12)):

$$\log K_{et} = \log K_{et}^0 + \frac{\alpha}{0.059}\left(E^0_{(M^{n+}/M^0)} - E_{CB}\right) \qquad (12)$$
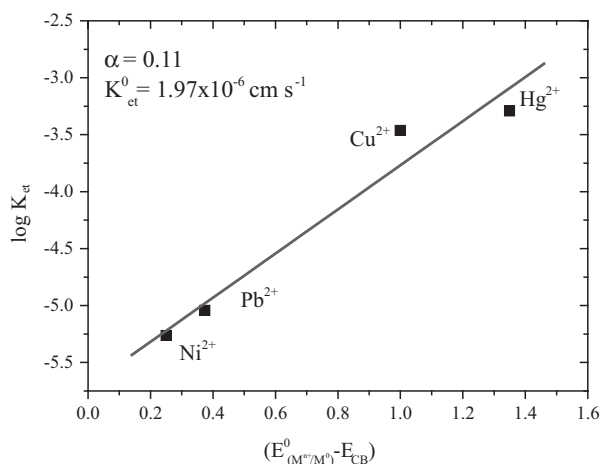
Figure 7 Relationship between interfacial electron transfer rates and the driving forces of the electron transfer reactions.

where α is the transfer coefficient and K_{et}^0 the value of the rate constant for $E_{(M^{n+}/M^0)}^0 - E_{CB} = 0$. The interfacial electron transfer rate constant K_{et} is given by

$$k_2' = 4\pi R^2 K_{et} \quad (R : \text{ sum of the radii of TiO}_2$$
$$\text{nanoparticle and the electron acceptor}) \quad (13)$$

where k_2' (cm^3 s^{-1}) is related to the observed second order rate constant k_2^{obs} (M^{-1} s^{-1}) by

$$k_2' = k_2^{obs} \times 1000/N_A \quad (N_A$$
$$= \text{the Avogadro's number}) \quad (14)$$

Table 2 summarizes the observed second order rate constants (k_2^{obs}) obtained from stopped flow kinetic data and the electron transfer rate constants (K_{et}) for electron transfer reaction of the studied metal ions reduction reactions. While no reaction between $e_{TiO_2}^-$ and Zn (II) or Mn (II) has been realized in our previous study due to thermodynamic infeasibility,[12] the results of the reduction of metal ions in the presented study show the expected trend concerning the relationship between log K_{et} and the driving force of the electron transfer reaction ($E_{(M^{n+}/M^0)}^0 - E_{CB}$) and taking the value $E_{cb}^0 = -0.5\ V_{NHE}$. This means that the electron transfer rate constants tend to increase with the driving force (Fig. 7).

4. Conclusions

In this study the reduction of hazardous metal ions Hg (II), Pb (II) and Ni (II) by the stored TiO$_2$ electrons ($e_{TiO_2}^-$) has been investigated. A steady state UV–vis absorption experiments were useful to determine the reactivity. It was found that the blue coloration of TiO$_2$ stored electrons ($e_{TiO_2}^-$) suspensions turned to yellow brawn, pale yellow or golden brawn coloration, respectively, immediately after mixing with aqueous solution of Hg (II), Pb (II) or Ni (II), respectively, with decay of $e_{TiO_2}^-$ absorbance and buildup of new absorption bands of the deposited metal particles. The deposited metal particles were found to be very sensitive to molecular oxygen. A partial or either complete oxidation of the particles is assumed to occur after exposure to oxygen. The reaction of these species with O$_2$ was indicated from the damping of their absorbance after purging with O$_2$.

A powerful stopped flow technique was used to study the dynamics of the electron transfer from TiO$_2$ nanoparticles to the heavy metal ions Hg (II), Pb (II) and Ni (II) in water. The results indicate that these metal ions are readily reduced by $e_{TiO_2}^-$ under our experimental conditions. The electron transfer rate constants were obtained by first order fitting to the transients decay at 600 nm. The transient absorbance buildup of deposited metal particles has been also followed. The observed electron transfer rates were found to increase with the metal ions concentrations. Moreover, the results of the reduction of metal ions in the presented study show the expected trend concerning the relationship between log K_{et} and the driving force of the electron transfer reaction.

References

Bahnemann, D.W., Henglein, A., Lili, J., Spanhel, L., 1984. Flash photolysis observation of the absorption spectra of trapped positive holes and electrons in colloidal titanium dioxide. J. Phys. Chem. 88, 709–711.

Bahnemann, D.W., Kormann, C., Hoffmann, M.R., 1987. J. Phys. Chem. 91, 3789–3798.

Cardenas, G., Tello, A., Segura, R., 2001. Synthesis and TEM studies of nickel colloids prepared in non aqueous solvents. Bol. Soc. Chil. Quim. 46, 441–446.

Chen, D.W., Ray, A.K., 2001. Removal of toxic metal ions from wastewater by semiconductor photocatalysis. Chem. Eng. Sci. 56, 1561–1570.

Creighton, J.A., Eadon, D.G., 1991. Ultraviolet–visible absorption spectra of the colloidal metallic elements. J. Chem. Soc. Faraday Trans. 87, 3881–3891.

Elango, G., Roopan, S.M., 2015. Green synthesis, spectroscopic investigation and photocatalytic activity of lead nanoparticles. Spect. Acta A 13, 367–373.

Henglein, A., Giersig, M., 2000. Optical and chemical observations on gold-mercury nanoparticles in aqueous solution. J. Phys. Chem. B 104, 5056–5060.

Jaerup, L., 2003. Hazards of heavy metal contamination. Br. Med. Bull. 68, 167–182.

Kapoor, S., Adhikari, S., Gopinathan, C., Mittal, J.P., 1999. Radiolytic production of metallic nanoclusters in a quaternary microemulsion system. Mater. Res. Bull. 34, 1333–1343.

Ketir, W., Bouguelia, A., Trari, M., 2008. Photocatalytic removal of M^{2+} (Ni^{2+}, Cu^{2+}, Zn^{2+}, Cd^{2+}, Hg^{2+} and Ag$^+$) over new catalyst CuCrO$_2$. J. Hazard. Mater. 158, 257–263.

Kormann, C., Bahnemann, D.W., Hoffmann, M.R., 1988. J. Phys. Chem. 92, 5196–5201.

Legrini, O., Oliveros, E., Braun, A.M., 1993. Photochemical processes for water treatment. Chem. Rev. 9, 671–698.

Litter, M.I., 1999. Heterogeneous photocatalysis. Transition metal ions in photocatalytic system. Appl. Catal. B 23, 89–114.

Litter, M.I., 2014. Mechanism of removal of heavy metals and arsenic from water by TiO$_2$-heterogeneous photocatalysis. Pure. Appl. Chem. 87, 557–567.

Meftah, A.M., Saion, E., Abd Moksin, M.M., Zainuddin, H.B., 2009. Absorbance of Nickel nanoparticles/polyaniline composite films prepared by radiation technique. Solid State Sci. Technol. 17, 167–174.

Meichtry, J.M., Dillert, R., Bahnemann, D.W., Litter, M.I., 2015. Langmuir 31, 6229–6236.

Metcalf and Eddy Inc, 1991. Wastewater Engineering Treatment, Disposal, and Reuse. McGraw-Hill, Inc New York.

Mohamed, H.H., Dillert, R., Bahnemann, D.W., 2011a. J. Photochem. Photobiol. A 217, 271–274.

Mohamed, H.H., Mendive, C.B., Dillert, R., Bahnemann, D.W., 2011b. J. Phys. Chem. A 115, 2139–2147.

Mohamed, H.H., Dillert, R., Bahnemann, D.W., 2011c. J. Phys. Chem. C 115, 12163–12172.

Mohamed, H.H., Dillert, R., Bahnemann, D.W., 2012. Chem. Eur. J. 18, 4314–4345.

Nguyen, V.N.H., Beydoun, D., 2003. Effect of formate and methanol on photoreduction/removal of toxic cadmium ions using TiO_2 semiconductor as photocatalyst. Chem. Eng. Sci. 58, 4429–4439.

Sadar, D., Neogi, S.K., Bandyopadhyay, S., Satpati, B., Ahir, M., Adhikary, A., Jain, R., Gopinath, C.S., Bala, T., 2015. Multi-faceted core-shell nanoparticles: superparamagnetism and biocompatibility. New J. Chem. 39, 8513–8521.

Salomons, W., Foerstner, U., Mader, P. (Eds.), 1995. Heavy Metals Problems and Solutions. Springer, p. 386.